Journal of Alloys and Compounds 509 (2011) 6222–6226

Contents lists available at ScienceDirect

Journal of Alloys and Compounds

journal homepage: www.elsevier.com/locate/jallcom

Synthesis and characterization of titanium doped sodium beta″-alumina

Xiaoling Wei, Yin Cao, Lei Lu, Hui Yang*, Xiaodong Shen

College of Materials Science and Engineering, Nanjing University of Technology, Nanjing 210009, China

ARTICLE INFO

Article history:
Received 5 November 2010
Received in revised form 3 March 2011
Accepted 3 March 2011
Available online 10 March 2011

Keywords:
TiO_2 doping
Na-β″-Al_2O_3
Solid electrolyte
Sodium–nickel chloride batteries

ABSTRACT

High dense Na–β″-Al_2O_3 electrolyte materials have been synthesized by solid state reaction with boehmite, magnesia, sodium carbonate and titania as the starting materials. The effects of TiO_2 doping percentage on the properties and microstructures of the prepared samples were investigated by X-ray diffraction (XRD), scan electron microscope (SEM), three point bending and ionic conductivity tests. The results indicated that both the relative densities and the phase purities of the samples could effectively improved after doping with TiO_2. The proper doping amount of TiO_2 was to form the transient liquid phase during the sintering process, which would reduce the steric effect and accelerate the diffusivity. Moreover, the mechanical performance of the obtained sample increased to the value above 280 MPa as the doping amount of TiO_2 was larger than 1 wt%. As to the electric properties, if the doping amount was less than 1 wt%, the grain boundary resistivity reduced as the density increased, so the ionic conductivity of the Na–β″-Al_2O_3 was enhanced obviously. However, when the doping amount was above 1 wt%, the ionic conductivity was deteriorated because of the increased resistivity caused by the broadening grain size.

1. Introduction

Low resistivity ionic conductor sodium–beta″-alumina has been extensively studied due to its applications in sodium–sulfur batteries [1–4] and sodium–nickel chloride batteries (ZEBRA batteries) [4,5]. Synthesis of sodium–beta″-alumina can be roughly categorized into two types: solid-state reaction processes and novel soft-chemistry routes such as sol–gel processing [6–8], co-precipitation [9], alkoxide hydrolysis [10], and solution combustion techniques [11], etc.

Even though the soft-chemistry methods could mix the reactants in the molecule-scale to ensure the high reactivity and thus to obtain the high quality products, it is generally difficult to scale up for industrial production. Therefore the solid-state reactions [12–19] without complicated process have attracted great attentions. The solid-state reactions have fallen into: (i) batch sintering [12]. Since the density has significant impact on the ionic conductivity and the mechanical property of the materials, a complete cycle of 24–36 h duration with a long sintering time at high temperature is essential to obtain the high density materials. (ii) Pass-through sintering [13]. It is also called zone-sintering [14]. This process has stringent requirements on the equipment and been reported mostly in 70–80s of last century [15–17]. As to the relatively easy batch sintering, in order to obtain high purity and dense β″-Al_2O_3, extensive researches have been carried out in recent years, including two-peak firing [18], partial synthesis method [19], etc.

Synthesis of sodium–beta″-alumina by conventional solid-state reaction inevitably requires a long holding time at a high sintering temperature. It leads to the loss of sodium, which must deteriorate the ionic conductivity seriously. Doping with certain oxides is supposed as an effective way to improve the properties of the conventional ceramic [16,20,21], such as densification [20–22], magnetic properties [23] and electrical properties [16,24–27]. Erkalfa et al. [20] reported that TiO_2 could promote the sintering process of alumina by enhancing the Al^{3+} diffusion due to the increasing concentration of the Al^{3+} vacancies. Zhang et al. [21], etc. also reported that doping levels of TiO_2 is beneficial to densification of Al_2O_3 and SiO_2 mixtures. Boilot and Thery [22] reported that the divalent cations with ionic radius <0.097 nm, such as Mg^{2+}, Ni^{2+}, Co^{2+}, Cu^{2+}, Zn^{2+}, Mn^{2+} and Cd^{2+}, were able to enter the spinel block to stabilize the β″ structure. These reports are consistent with the theory of titanium substituting for aluminium in the spinel blocks [14,28]. In May's work [16], the influence of barium and titanium dopants on the ionic conductivity and phase composition of sodium–beta-alumina was reported, in which the sodium–beta-alumina was formed by isostatic pressing and was sintered at 1990 K in a pass-through furnace with a speed of 35 mm/min. But the influence of TiO_2 as a single dopant on sodium–beta″-alumina has not been reported yet.

In this paper, we investigated the doping effects of TiO_2 on the mechanical and electrical properties of synthesized Na–β″-Al_2O_3 electrolytes by X-ray diffraction, scan electron microscopy, three-

* Corresponding author. Tel.: +86 25 83587238; fax: +86 25 83587238.
E-mail address: yanghui@njut.edu.cn (H. Yang).

0925-8388/$ – see front matter © 2011 Elsevier B.V. All rights reserved.
doi:10.1016/j.jallcom.2011.03.006

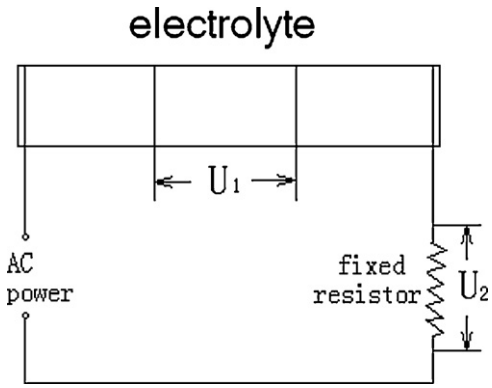

Fig. 1. The schematic diagram of ionic conductivity measurement by a 4-terminal method.

point intensity testing and AC 4-probe method respectively. The purpose of doping TiO_2 is to improve the sintering behavior, tailor the microstructure, and enhance the mechanical properties.

2. Experimental

2.1. Synthesis of Na–β″-Al_2O_3 solid electrolytes

Na–β″-Al_2O_3 solid electrolytes doped with TiO_2 are synthesized via a solid state reaction using commercial powders of boehmite, magnesia, sodium carbonate and titania as the starting materials. Boehmite is calcined at 1150 °C for 2 h to obtain the precursor. The doping amount of TiO_2 increases from 0.5 to 2 wt% with 0.25 wt% as the interval. Compositions of various Na–β″-Al_2O_3 ceramics used in this investigation is designated with the sample codes of A0–A7, respectively. The mixture is ball-milled in an absolute alcohol medium for 8 h with the fixed rotation speed of 400 rpm. After the slurries are dried and mixed with an appropriate amount of 5 wt% polyvinyl alcohols, the powders are ground to <180 mesh in an alumina mortar. The resulting mixtures are then molded by the uniaxial stress of 200 MPa to obtain the green samples in two sizes: 5 mm × 7 mm × 60 mm and ϕ18 mm × 2 mm. Without the cold isotropic pressing process, the green samples are packed in a Pt-crucible and heated to 1580 °C for 15 min in a Si–Mo stove (Wanyuan electric stove co., ltd. CGME-14-180) with the heating rate of 10 °C/min. In order to accelerate the formation of β″-Al_2O_3, a 4 h holding time at 1450 °C in the cooling process is added.

2.2. Characterization of Na–β″-Al_2O_3 solid electrolytes

Densities of the sintering samples are measured by an absolute density technology using the micromeritics Accupyc || 1340 Pycnometer with the N_2 pressure of 20 psi. To determine their phase compositions, X-ray diffractometer (XRD) (Rigaku, Japan) analysis is carried out for all the samples with Cu Kα radiation (λ = 1.5406 Å) operating at 40/40 kV/mA. The scanning speed is 5°/min and the 2θ ranges from 5° to 75°. The relative ratio of Na/β-Al_2O_3 and Na/β″-Al_2O_3 are quantitative calculated using the normalized index, according to Alina Pekarsky's formula f(β) [29].

$$f(\beta'')\% = 100 - f(\beta)\% = 100 - \frac{1.14I_{\beta}}{1.14I_{\beta}+I_{\beta''}} \times 100 \quad (1)$$

where $I_{\beta''}$ and I_{β} are the peak intensities at 45.90° and 44.50°, respectively.

The microstructure of the resultant ceramics is observed by a QUANTA 200 scanning electron microscope (SEM). The specimens are polished with 1 μm diamond paste, and then thermally etched at 1500 °C for 10 min in air for SEM observations. The particle sizes are calculated by an image analyzer taken from at least 300 grains.

Bending strength measurements are performed in three point bending (span 30 mm) on rectangular sintered specimens with cross-section of 3 mm × 5 mm. The surfaces of all samples are polished with SiC sandpapers and diamond pastes down to 0.25 μm, and followed by the annealing to eliminate the possible surface stress which is induced during the grinding processes. After 0.5 mm/min indenter loading, the crack load F is measured by the Electronic Universal Testing Machine (CMT 6203). Bending strength is calculated by the following formula:

$$\sigma = \frac{3FL}{2BH^2} \quad (2)$$

where σ is bending strength (MPa), F is the crack load (N), L is the span of the specimen (mm), B is the width of the specimen (mm) and H is the height of the specimen (mm).

The ionic resistivity is measured using a simple AC four-terminal method [15] (Fig. 1). Four Ni wires are wrapped tightly around the circumferemce of the sample spaced along its length. The outer 2 act as the current connections and the inner 2 are for measuring the voltage. A salt mixture solution is dropped to each loop to ensure a good ionic connection. The mixed solution is composed of sodium nitrite and sodium nitrate in eutectic proportions. Around 8 V AC are applied to the circuit containing a 1000 Ω resistor in series with the outer nickel terminals to the ceramic sample. The voltages across the inner nickel terminals and across the 1000 Ω resistor are measured by a digital multimeter (Keithley 2000). The measure temperature is raised to and cooled from 500 °C to 200 °C with 50 °C interval. At each temperature a value for the resistivity is calculated using the values for voltage, CSA (cross-sectional area) and the length of inner 2 wires (formula (3)).

$$\rho = \frac{1000 \times U_1 \times CSA}{U_2 \times L} \quad (3)$$

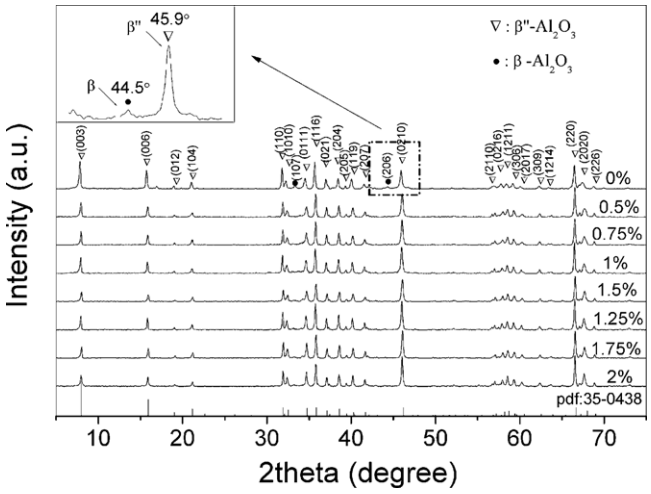

Fig. 2. X-ray diffraction patterns of specimens with different amounts of TiO_2 doping.

3. Results and discussion

3.1. XRD analysis

Fig. 2 shows the typical X-ray diffraction patterns of the samples doping with different amounts of TiO_2 sintered at 1580 °C for 15 min. The XRD patterns of all samples conform to the crystalline phase of $Na_{1.67}Mg_{0.67}Al_{10.33}O_{17}$ (JCPDS 35-0438). The enlarged inset exhibits the details from 42 to 48° where the characteristic peaks of β″ phase and β phase could be clearly clarified. In addition, the ratio of the β″ phase could be calculated according to the Eq. (1) and the obtained results are listed in Table 1. With the dopants increasing from 0 to 2.0 wt%, the content of β″ phase increases and the patterns are more intensive. As for the diffraction patterns corresponding to TiO_2, no significant peaks were detected, which may be due to its low concentration(less than 2 wt%). Except for the contents of β″ phase, all the critical grain sizes were measured via SEM, and relative densities were determined by the absolute density technology of all samples are also shown in Table 1.

The doped TiO_2 improves the purity of the specimens effectively. According to Boilot and Thery's theory [22], Ti^{4+} ($r_{Ti^{4+}}$ = 0.068 nm < 0.097 nm) is able to enter the spinel block to stabilize

Table 1
Critical grain size, content of β″ phase and relative density of synthesized Na–β″-Al_2O_3 ceramics with various TiO_2 doping.

Sample	TiO_2 (wt%)	Critical grain size (μm)	Content of β″-Al_2O_3 (%)	Relative density (%)
A0	0.0	1.08	95.2	89.4
A1	0.5	1.44	95.9	94.5
A2	0.75	1.48	96.2	95.4
A3	1.0	1.59	97.5	96.2
A4	1.25	1.69	97.1	96.8
A5	1.5	1.77	97.9	97.2
A6	1.75	1.81	98.1	98.6
A7	2.0	1.85	97.7	97.8

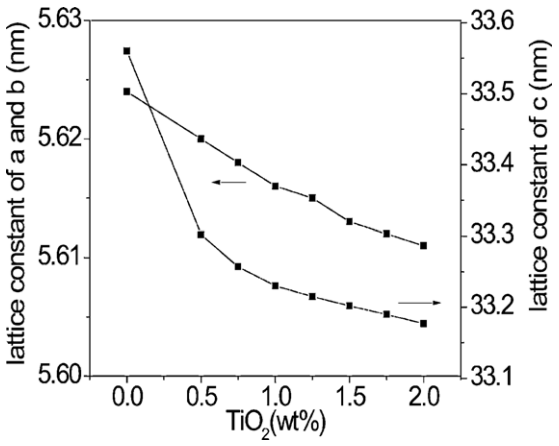

Fig. 3. The calculated lattice constant of specimens with different amounts of TiO_2 doping.

the β″ structure. This may be explained through that Ti^{4+} occupied Al^{3+} positions in the spinel block [16], enhancing the diffusivity of the aluminium-ion sequentially stabilizing the β″ structure. With the increase of the dopant, the ratio of β″ phase rises. This trend is consistent with the theoretics of Boilot and Thery.

Though the diffraction patterns corresponding to Titanium have not been detected by XRD patterns due to its low concentration (less than 2 wt%), the effect of doping to the lattice constant could not be ignored. Fig. 3 shows the changes of lattice constant of samples with different amount of TiO_2. As illustrated in Fig. 3, with the increase of the TiO_2 content, both the in-plane parameter a and the interlayer spacing c decreased. Since Ti^{4+} is able to enter the spinel block [22], the changing of the lattice constant observed in Fig. 3 can be attributed to the different ionic radius of element and the electrostatic effects.

3.2. SEM and EDS analysis

Fig. 4 shows the SEM images of the Na–β″-Al_2O_3 doped with different amounts of TiO_2. The undoped sample possesses loose structure with irregular fine grains. After doping, the densification of material is improved. Though the specimens containing 0.50 wt% and 0.75 wt% TiO_2 are denser, there are still some inhomogeneous zones with partially plump grains and certain holes, especially the 0.5 wt% TiO_2 sample. As the amount of dopant increases from 1.0 to 2.0 wt%, the trends of accelerating the growth of grains and improving the relative density become more evident. However, the excessive grain growth is obvious in the 1.75 wt% and 2.00 wt% TiO_2 samples. If the exaggerated grains are massive, the ionic conductivity of the material will be significantly deteriorated.

Combined with the data in Table 1, the relative density of undoped sample is only 89.4%. The densities of doped composites are obviously higher than that of un-doped sample. When the content of the dopant is above 1.5 wt%, all the relative densities of the samples exceed 97%. This indicates the doping TiO_2 effectively improves the densification of materials. The other important result of doping is accelerating the growth of grains of the sample. Table 1 demon-

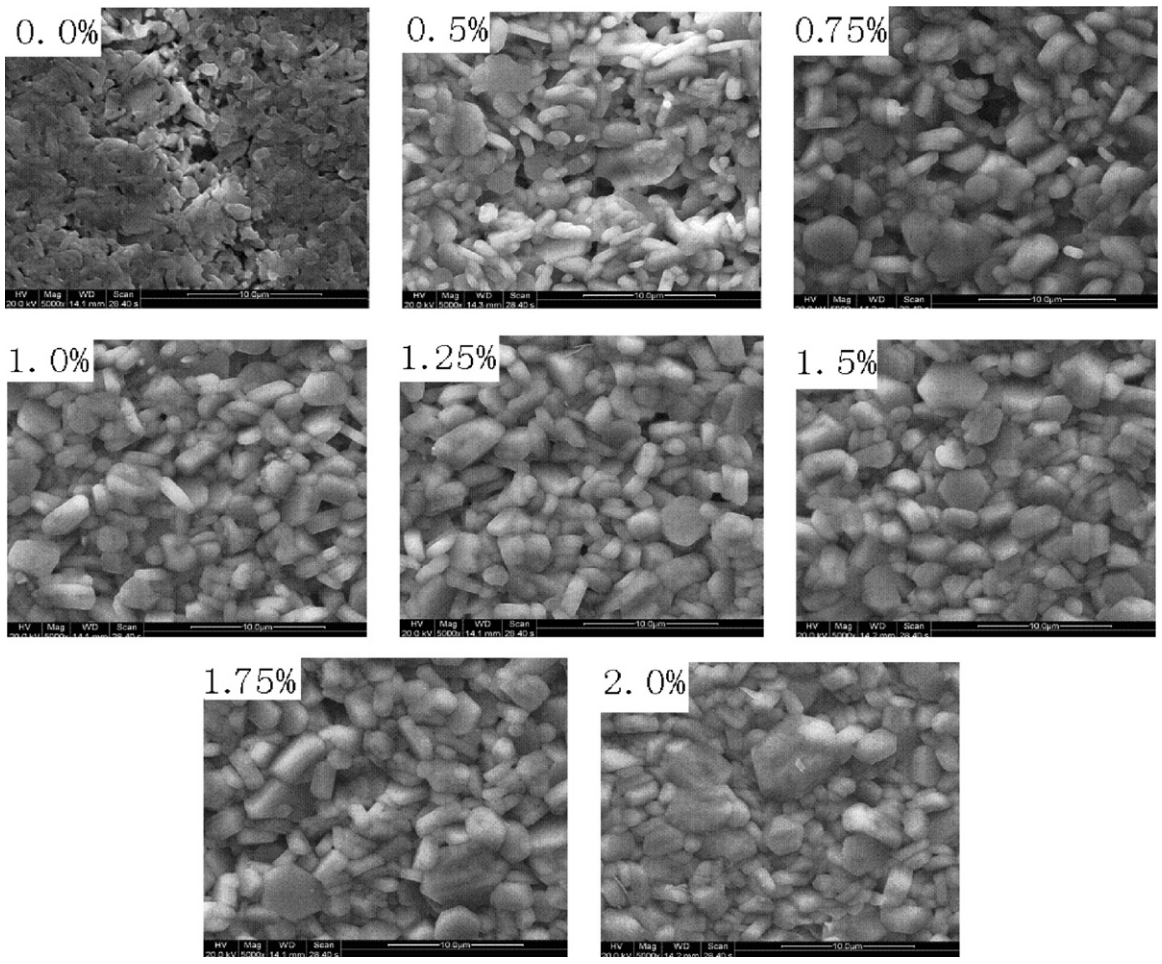

Fig. 4. SEM of the Na–β″-Al_2O_3 doped with different contents of TiO_2.

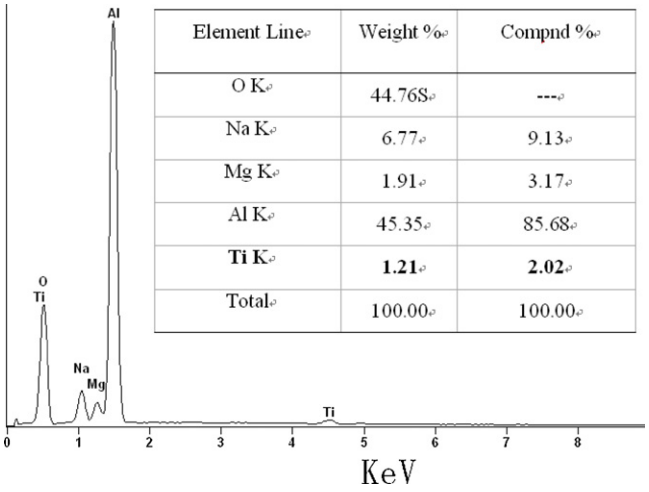

Element Line	Weight %	Compnd %
O K	44.76S	---
Na K	6.77	9.13
Mg K	1.91	3.17
Al K	45.35	85.68
Ti K	**1.21**	**2.02**
Total	100.00	100.00

Fig. 5. EDS analysis of sintered sample with 2 wt% TiO_2.

strates that the grain size of specimen grows up as the dopant increases. This is consistent with the SEM images. It suggests that TiO_2 promotes the sintering process of the Na–β″-Al_2O_3, accelerates the growth of grains and improves density of materials. This may be attributed to the mechanism that the TiO_2 could enhance the diffusivity of the aluminium-ion and reduce the steric effect due to the intergranular transient liquid phase [30,31]. As a result, the grains could rearrange themselves to form the high densification.

As for the amounts of TiO_2 dopants are traceable, the XRD patterns of impurity phases have not been detected. But the result from EDS analysis reveal the existence of Titanium. It can be seen in Fig. 5, EDS analysis of sintered sample with 2 wt% TiO_2, the detected content of TiO_2 is 2.02 wt%, close to its theoretical ratio of 2 wt%.

3.3. Strength analysis

Fig. 6 shows the relationship of the amounts of TiO_2 and the bending strength of the samples. The bending strength of the specimen is enhanced obviously with the increase of the dopant. When the content of dopant achieves to 1.00 wt%, the bending strength of the specimens exceeds 280 MPa, while the bending strength of un-doped sample is only 210 MPa at the same condition.

According to the XRD patterns and the SEM images, the crystalline contents and the densities of the specimens are obviously improved with the increase of dopant. As mentioned above, the steric effect is reduced due to the transient liquid phase. As a result, the grain rearrangement is enhanced and the bending strength is improved.

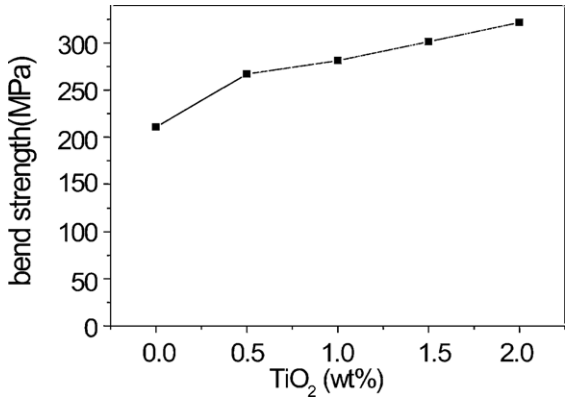

Fig. 6. Bending strength of specimens doped with different amounts of TiO_2.

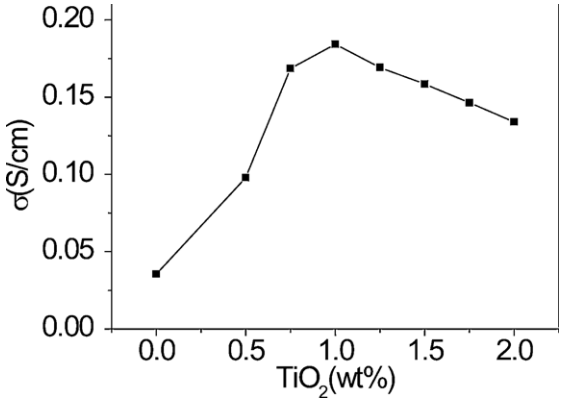

Fig. 7. Ionic conductivities of specimens with different additives at 300 °C.

3.4. Ionic conductivity analysis

Fig. 7 shows the ionic conductivity of samples with different amounts of TiO_2 doping at 300 °C. As we know, the ionic conductivity is determined by the grain resistance and the boundary resistance. The ionic conductivity of un-doped sample is low due to its loose structure which increases the grain boundary resistance. With the doping amount increasing (≤1 wt%), the sample becomes denser which will reduce the grain boundary resistance. As a result, the ionic conductivity of the sample improves dramatically. However, the ionic conductivity declines when the amounts of TiO_2 dopants are above 1 wt%. Combined with the SEM images and Table 1, the grain size of specimen increases with the increase of TiO_2 amount, which causes the grain resistance exaggerated. Doubtlessly, the ionic conductivity is deteriorated.

The activation energy for ionic migration, E_a, which is an important parameter to judge the sintering property of the material. Fig. 8 is the relationship of the ionic conductivity and the temperature of the 1 wt% TiO_2 sample. The relationship obeyed Arrnhenius equation (4) [32]. According to the equation, we could calculate the activation energy of the sample.

$$\sigma = \frac{\sigma_0}{T} \exp\left(-\frac{E_a}{RT}\right) \tag{4}$$

R is the gas constant, T is the absolute temperature, σ_0 is a constant. As showed in Fig. 8, when the temperature is above 300 °C, the activation energy declines from 0.47 eV to 0.25 eV. It demonstrates that with the increase of temperature, the resistance of Na^+ ion conduction decreases significantly. As a result, the mobile speed is improved. This phenomenon is consistent with the trend of Na^+ ion conductivity improved with the increase of temperature [33].

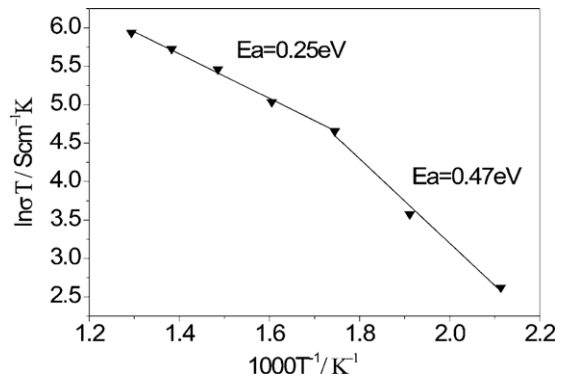

Fig. 8. Relationship of the temperature and conductivity of Na–β″-Al_2O_3 (1 wt% TiO_2).

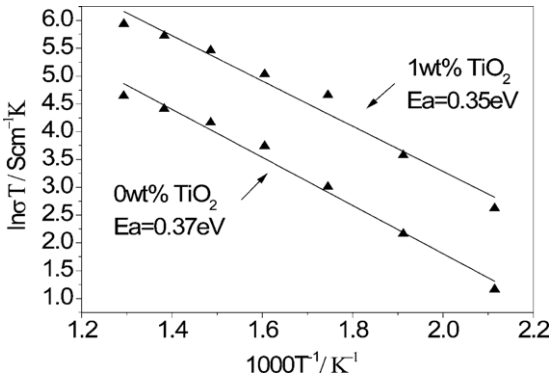

Fig. 9. Arrhenius plot of resistivity data for samples of un-doped sample and 1 wt% TiO_2 sample.

Arrhenius plot of resistivity data measured between 573 and 773 K are shown in Fig. 9. The corresponding values for the activation energies are 0.37 eV and 0.35 eV for undoped sample and doping sample with 1 wt% TiO_2, respectively. Compared to the undoped sample, the 1 wt% TiO_2 sample exhibits a lower E_a. The lower E_a signifies the convenient ionic migration. The low activation energy is attributed to the intergranular transient liquid phase at high temperature. The liquid phase could reduce the steric effect. Maybe this is the key factor to the smaller activation energy.

4. Conclusions

With the raw materials of boehmite, Na_2CO_3, MgO and the dopant TiO_2, Na–β″-Al_2O_3 electrolyte materials are synthesized by the conventional solid state reaction. The obtained results indicates that the doped TiO_2 plays an important role in promoting the sintering process of Na–β″-Al_2O_3 electrolyte. All the β″ phase percentages of doped samples are above 96%. The samples with 1–1.5 wt% doping possess uniform microstructure with dense and plump grains. The bending strength of the doped sample is enhanced obviously with the increase of the dopant content. When the content of TiO_2 is above 1 wt%, the bending strength exceeds 280 MPa. Adding a small amount of TiO_2 can refine particle sizes, improve the density, reduce grain boundary resistance so as to increase sample conductivity. Nevertheless, the excessive TiO_2 will accelerate the growth of abnormal grains and increase the grain resistance. As a result, the sample conductivity is deteriorated. This will result in a negative effect on their application in energy storage batteries. Therefore, the optimal amount of TiO_2 doping in this study is determined as 1 wt%.

Acknowledgements

The authors would like to thank the financial support from National Natural Science Funds (2007CB209705), and the kindly help from Miss Huang and Mr. Qian for SEM and XRD analysis.

References

[1] P.W. Mcgeehin, A. Hooper, J. Mater. Sci. 12 (1977) 1.
[2] Z. Wen, J. Cao, Z. Gu, Solid State Ionics 179 (2008) 1697.
[3] Z. Wen, Z. Gu, X. Xu, J. Power Sources 184 (2008) 641.
[4] X. Lu, G. Xia, J.P. Lemmon, Z. Yang, J. Power Sources 195 (2010) 2431.
[5] J. Prakash, L. Redey, D.R. Vissers, J. Power Sources 87 (2000) 195.
[6] R. Subasri, Tom. Mathews, O.M. Sreedharan, V.S. Raghunathan, Solid State Ionics 158 (2003) 199.
[7] L. Ning, W. Zhaoyin, W. Xiangwei, Z. Jingchao, L. Yu, J. Alloys Compd. 479 (2009) 648.
[8] W. Jin, J. Xiaoping, W. Xiaoling, Y. Hui, S. Xiaodong, J. Alloys Compd. 497 (2010) 295.
[9] H.C. Park, Y.B. Lee, S.G. Lee, C.H. Lee, J.K. Kim, S.S. Hong, S.S. Park, Ceram. Int. 31 (2005) 293.
[10] P.E.D. Morgan, Mater. Res. Bull. 11 (1976) 233.
[11] T. Mathews, Mater. Sci. Eng. B 78 (2000) 39.
[12] Hames M.D., Duncan J.H., Society of automotive engineers congress, 1975, Paper 750375.
[13] S.R. Tan, G.J. May, Sci. Ceram. 9 (1977) 103.
[14] J. Wynn, L.J. Miles, Proc. Br. Ceram. Soc. 19 (1971) 161.
[15] G.J. May, J. Mater. Sci. 13 (1978) 261.
[16] G.J. May, J. Mater. Sci. 14 (1979) 1502.
[17] R. Stevens, J.G.P. Binner, J. Mater. Sci. 19 (1984) 695.
[18] J.H. Duncan, W.G. Bugden, Proc. Br. Ceram. Soc. 31 (1981) 221.
[19] C. Kungang, L. Zuxiang, J. Inorg. Mater. 12 (1997) 725.
[20] H. Erkalfa, Z. Misirli, T. Baykara, Ceram. Int. 24 (1998) 81.
[21] T.S. Zhang, L.B. Kong, Z.H. Du, J. Ma, S. Li, J. Alloys Compd. 506 (2010) 777.
[22] J.P. Boilot, J. Thery, Mater. Res. Bull. 11 (1976) 407.
[23] D. Guo-Ping, H. Zhi-Juan, H. Qi-Feng, Q. Xiao-Mei, S. Wang-Zhou, J. Alloys Compd. 492 (2010) L79.
[24] J. Yuan, L. Jiang, H. Tianmin, W. Jinxia, S. Wenhui, J. Alloys Compd. 389 (2005) 317.
[25] L. Ming-long, Y. De-an, Q. Yuan-fang, J. Alloys Compd. 496 (2010) 449.
[26] X.P. Jiang, Y. Chen, K.H. Lam, S.H. Choy, J. Wang, J. Alloys Compd. 506 (2010) 323.
[27] F. Hai, P. Zhijian, F. Xiuli, F. Zhiqiang, W. Chengbiao, Q. Longhao, M. Hezhuo, J. Alloys Compd. 497 (2010) 304.
[28] E.S. Lugovskaya, V.N. Pavlikov, V.A. Artemov, N.L. Korobanova, Inorg. Mater. 12 (1976) 1520.
[29] A. Pekarsky, P.S. Nicholson, Mater. Res. Bull. 15 (1980) 1517.
[30] K. Hamano, C.S. Hwang, Z. Nakagawa, Y. Ohya, Yogyo Kyokaishi, Jpn. Ceram. 94 (5) (1986) 505.
[31] C.-J. Wang, C.-Y. Huang, Mater. Sci. Eng. A 492 (2008) 306.
[32] Z. Wen, Z. Lin, Z. Gu, X. Xu, D. Jiang, J. Inorg. Mater. 18 (2003) 1313.
[33] Chen. Kungang, Xu. Xiaohe, Lin. Zuxiang, J. Inorg. Mater. 12 (1997) 521.